HHS Public Access

Author manuscript

Curr Cardiol Rep. Author manuscript; available in PMC 2017 July 11.

Published in final edited form as:

Curr Cardiol Rep. 2017 April ; 19(4): 33. doi:10.1007/s11886-017-0843-0.

Recent Advances and Clinical Applications of PET Cardiac Autonomic Nervous System Imaging

Nabil E. Boutagy[1] and **Albert J. Sinusas**[1,2]

[1]Section of Cardiovascular Medicine, Department of Medicine, Yale University School of Medicine, 375 Congress Avenue, New Haven, CT 06519, USA

[2]Department of Radiology and Biomedical Imaging, Yale University School of Medicine, New Haven, CT, USA

Abstract

Purpose of Review—The purpose of this review was to summarize current advances in positron emission tomography (PET) cardiac autonomic nervous system (ANS) imaging, with a specific focus on clinical applications of novel and established tracers.

Recent Findings—[^{11}C]-Meta-hydroxyephedrine (HED) has provided useful information in evaluation of normal and pathological cardiovascular function. Recently, [^{11}C]-HED PET imaging was able to predict lethal arrhythmias, sudden cardiac death (SCD), and all-cause mortality in heart failure patients with reduced ejection fraction (HFrEF). In addition, initial [^{11}C]-HED PET imaging studies have shown the potential of this agent in elucidating the relationship between impaired cardiac sympathetic nervous system (SNS) innervation and the severity of diastolic dysfunction in HF patients with preserved ejection fraction (HFpEF) and in predicting the response to cardiac resynchronization therapy (CRT) in HFrEF patients. Longer half-life ^{18}F-labeled presynaptic SNS tracers (e.g., [^{18}F]-LMI1195) have been developed to facilitate clinical imaging, although no PET radiotracers that target the ANS have gained wide clinical use in the cardiovascular system. Although the use of parasympathetic nervous system radiotracers in cardiac imaging is limited, the novel tracer, [^{11}C]-donepezil, has shown potential utility in initial studies.

Summary—Many ANS radioligands have been synthesized for PET cardiac imaging, but to date, the most clinically relevant PET tracer has been [^{11}C]-HED. Recent studies have shown the utility of [^{11}C]-HED in relevant clinical issues, such as in the elusive clinical syndrome of HFpEF. Conversely, tracers that target cardiac PNS innervation have been used less clinically, but novel tracers show potential utility for future work. The future application of [^{11}C]-HED and newly designed ^{18}F-labeled tracers for targeting the ANS hold promise for the evaluation and management of a wide range of cardiovascular diseases, including the prognostication of patients with HFpEF.

Correspondence to: Albert J. Sinusas.

Conflict of Interest Nabil E. Boutagy and Albert J. Sinusas declare that they have no conflict of interest.

Compliance with Ethical Standards

Human and Animal Rights and Informed Consent This article does not contain any studies with human or animal subjects performed by any of the authors.

Keywords

Positron emission tomography; Autonomic nervous system; Imaging; Cardiovascular disease

Introduction

The autonomic nervous system (ANS) controls most visceral functions of the body independent of voluntary control [1, 2]. Specifically, the ANS participates in exclusive or partial control over cardiovascular, respiratory, gastrointestinal, and urinary functions. The ANS is able to transmit autonomic signals to and from visceral organs via efferent and afferent neurons, respectively. These autonomic signals are sent through two major subdivisions called the sympathetic nervous system (SNS) and the parasympathetic nervous system (PNS) that exert control over target organs via the direct release of neurotransmitters that act on target cells or the indirect release of hormones and other effector molecules [1, 2].

The ANS plays a key role in maintaining cardiovascular homeostasis at rest and in response to a variety of stimuli (e.g., exercise and postural changes) by regulating cardiac output, vasoreactivity, and metabolism [3]. It has been recognized that aberrations in either ANS subdivision, due to aging and other chronic stressors, contribute to pathobiology of many cardiovascular diseases, including hypertension, ischemic heart disease (IHD), and heart failure (HF) and portend worse cardiovascular prognosis in many of these diseases [4–7]. The assessment of the ANS activity through reflex testing or circulating biomarker measurements are non-specific to the heart and may reflect off target pathologies [8]. In contrast, radiotracer analogs that target pre- and postsynaptic SNS and PNS receptors allow for the direct evaluation of cardiac ANS innervation and function and have been useful in characterizing the influence of the ANS in many cardiovascular diseases. Single photon emission tomography (SPECT) analogs of nor-epinephrine, specifically ^{123}I-metaiodobenzylguanidine (^{123}I-mIBG), have been well characterized and studied [8–10]. As such, ^{123}I-mIBG SPECT imaging for the assessment of HF prognosis has recently been approved by the Food and Drug Administration (FDA). However, the cost of these scans has been prohibitive to wide diagnostic use of this agent. Positron emission tomography (PET) offers several advantages over SPECT imaging, including higher spatial resolution and established quantitative methods. In addition, a larger variety of ANS radiotracers exist for PET compared to SPECT imaging and thus allow for more extensive evaluation of cardiac ANS function. This review highlights advances in PET cardiac ANS imaging, with a specific focus on the clinical applications of novel and established tracers in relevant cardiovascular disease models.

Cardiac Sympathetic Nervous System Imaging

Activation of the SNS has mainly stimulatory actions on the heart that include increased chronotropism, dromotropism, bathmotropism, and inotropism [2]. The sympathetic pathway to the heart originates from preganglionic neurons in the intermediolateral horn of the spinal cord at the level of T1–T5, and synapse with postganglionic neurons within the

sympathetic nerve chain. The postganglionic neurons, specifically the cardiac cervical and thoracic nerves, arrive at cardiac plexus and give rise to sympathetic efferents that innervate the atria and ventricles, the conduction system, and the coronary arteries [1, 2].

Postganglionic SNS nerve endings release stored norepi-nephrine (NE) from secretory vesicles following an action potential and nerve depolarization for subsequent binding to adrenergic, G protein-coupled receptors on effector cells. The adrenergic receptors are broken into the subtypes α and β, with the subtypes α_1, β_1, and β_2 being the predominant isoforms in the cardiovascular system [11]. After release, most of the NE in the synaptic space (50–80%) is removed by reuptake by the presynaptic nerve terminal via the NE reuptake transporter (NET or uptake-1) in an energy-dependent manner [1]. The majority of the reabsorbed NE is repacked into secretory vesicles by vesicular monoamine transporter (VMAT), while a small portion is metabolized by monoamine oxidase (MAO) and catechol-O-methyltransferase (COM) [1]. The remaining NE is taken up in postsynaptic cells by the energy-independent, uptake-2 mechanism, or by diffusion into the vascular space (Fig. 1). Clinically available and experimental SNS PET imaging radioligands mainly target presynaptic neural activity (e.g., uptake-1 and metabolism) and postsynaptic adrenergic receptor density. Below is a current description of experimental and clinically relevant PET imaging agents that provide non-invasive, in vivo information of SNS cardiac innervation.

Tracers of SNS Presynaptic Nerve Activity

[^{11}C]-Meta-hydroxyephedrine (HED) has been well characterized in cellular [12•], animal [13], and human [14] studies and is the most routinely used PET imaging agent for SNS nerve activity. [^{11}C]-HED is a metabolically resistant analog of NE. [^{11}C]-HED has a high binding affinity (K_i = 20.9 nM) [15] and selectivity (~90%) [13, 16, 17] for myocardial uptake-1, is partially repacked upon uptake, and released back into synaptic space by passive diffusion or active release with endogenous NE. Therefore, the retention of [^{11}C]-HED represents continual recycling of the tracer by the presynaptic neuron [13]. Tracer distribution in the myocardium is regionally homogenous and produces excellent image quality due to rapid blood clearance and slow myocardial clearance (half-time, ~4 h) [14, 18]. Myocardial [^{11}C]-HED uptake is typically quantified non-invasively as the retention of radioactivity in the myocardium at the end of a dynamic scan, over the integral of the image-derived arterial input function (retention index [RI]). Although [^{11}C]-HED RI has been shown to be clinically diagnostic of SNS denervation, it is worth noting that metabolite analysis has shown significant accumulation of [^{11}C]-labeled metabolites in the blood after injection of [^{11}C]-HED in rodents and in humans [14, 19]. [^{11}C]-HED appears to be only peripherally metabolized, with greater than 99% authentic [^{11}C]-HED in the myocardium 30 min after injection [16, 17, 19]. Notwithstanding the frequent use of semi-quantitative measures, this tracer has been immensely valuable in evaluating SNS innervation in many cardiovascular diseases and continues to provide biomedical researchers with valuable and predictive information (see below).

[^{11}C]-Epinephrine (EPI), a true neurotransmitter, was developed to more closely resemble biochemical handling of NE with respect to neuronal uptake, vesicular storage, and intraneuronal metabolism [20]. Raffel has reported high binding affinity for human NET (K_i

= 68.4 μM [12•]) similar to NE, while others have shown high specificity for myocardial uptake-1 (~90%) and vesicular transport (95%) [20]. Notably, [^{11}C]-EPI retention in the myocardium is not influenced by continual reuptake at the presynaptic cleft as is [^{11}C]-HED [13]. [^{11}C]-EPI produces clear images due to rapid blood clearance and very slow myocardial clearance (half-time, ~10 h) [14]. Stable retention in the myocardium indicates efficient vesicular uptake and protection of [^{11}C]-EPI from intraneuronal metabolism [21•]. As such, the [^{11}C]-EPI RI is higher than that observed for [^{11}C]-HED in humans [14, 21•]. However, peripheral metabolism of [^{11}C]-EPI necessitates the need for metabolite correction even for simple RI calculations. It is important to note that species differences exist with respect to myocardial [^{11}C]-EPI washout, and caution must be taken when applying findings in rodents to humans [13].

[^{11}C]-Phenylephrine (PHEN) is synthetic catecholamine with an intermediate capacity for vesicular storage (> [^{11}C]-HED, but <[^{11}C]-EPI) [22]. [^{11}C]-PHEN is highly susceptible to intraneuronal MAO degradation and has a lower binding affinity for the uptake-1 mechanism (K_i = 109 nM [15]) compared to both [^{11}C]-HED and [^{11}C]-PHEN, resulting in rapid myocardial washout and comparatively lower retention than the aforementioned tracers [23]. Similarly to [^{11}C]-EPI, retention in the myocardium is not influenced by continual reuptake at the presynaptic cleft [13]. Taken together, the RI of [^{11}C]-PHEN, after plasma metabolite correction, has been used as in vivo index of presynaptic neuronal MAO activity. However, MAO is not only present on SNS presynaptic neurons, and thus, the production of extra-neuronal [^{11}C]-PHEN metabolites obscures interpretation of the myocardial RI.

Dopamine is an endogenous neurotransmitter that has a high binding affinity (K_i = 8.1 (μM) and transport kinetics (K_m = 0.24 μM) to human NET [12•]. Dopamine is the substrate for VMAT vesicular packing and converts to NE within the presynaptic neuron, and is susceptible to intra- and extra-neuronal metabolism. 6-[^{18}F]-Fluorodopamine (6F-DA) exhibits similar uptake/release kinetics and metabolism to endogenous dopamine [24]. As such, cardiac [^{18}F]-6 F-DA uptake and washout was proposed to represent sympathetic innervation and function [25]. However, low myocardial uptake-1 selectively (~50–60%) combined with the complex fate of [^{18}F]-6 F-DA rendered kinetic modeling difficult and precluded absolute quantification and widespread use of this tracer.

[^{18}F]-LMI1195

(^{18}F-N-[3-Bromo-4-(3-Fluoro-Propoxy)-Benzyl] -Guanadine)

To overcome the challenges in applying [^{11}C]-labeled PET SNS radiotracers, an [^{18}F]-labeled benzylguanidine, ^{18}F-*N*-[3-bromo-4-(3-fluoro-propoxy)-benzyl]-guanadine ([^{18}F]-LMI1195), was developed to resemble the structure of ^{123}I-mIBG and take advantage of high sensitivity PET imaging and the longer half-life of [^{18}F] [26]. [^{18}F]-LMI1195 has similar binding affinity and transport kinetics to endogenous NE for human NET [26] and similar tracer kinetics to ^{123}I-mIBG [27, 28]. Initial studies showed relatively high myocardial selectively for the uptake-1 mechanism in rabbits (82%) and in non-human primates (66%) [26]. These initial studies also showed excellent image quality of [^{18}F]-LMI1195 that was superior to^{123} I-mIBG. Sinusas et al. [29••] performed the first-in-human safety, toxicity, biodistribution, and dosimetry studies with [^{18}F]-LMI1195. This

preliminary, multi-center study showed patient safety and tolerability, acceptable dosimetry, and uptake and clearance kinetics favorable for myocardial imaging. In particular, blood radioactivity cleared quickly, whereas myocardial uptake remained stable over a 5-h imaging session. In addition, liver and lung radioactivity cleared relatively quickly, providing a very favorable target-to-background ratio for cardiac imaging (Fig. 2). Importantly, these studies reported significant metabolism of [^{18}F]-LMI1195 over time, which will need to be considered for quantification of [^{18}F]-LMI1195 images in the future. Despite these initial favorable findings, the clinical application of [^{18}F]-LMI1195 for SNS presynaptic neuron imaging has not progressed.

Tracers of Postsynaptic SNS Receptors

Cardiac β-Adrenergic Receptor PET Imaging

β_1 and β_2 are the predominant β-receptors in the heart and are linked to G_s proteins that when activated will cause an increase in adenylyl cyclase activity that causes an increase in cyclic adenosine monophosphate (cAMP) (Fig. 1) [1, 11]. Activation of cAMP has stimulatory actions on cardiomyocytes and leads to smooth muscle relaxation (vasodilation) in the coronary vasculature. β_1 and β_2 receptors are evenly distributed in all four chambers, and in the normal heart, the β_1/β_2 ratio is approximately 3:1 [11]. As discussed in more detail below, there is a complex relationship between SNS nerve activity, β-adrenoceptor expression and activity, and cardiac disease. Two PET radioligands that bind to β-adrenoceptor non-selectively have undergone significant preclinical testing with translation to clinical evaluation.

[^{11}C]-CGP-12177 is the most widely used PET tracer for postsynaptic adrenergic imaging and is a hydrophilic, non-selective β-antagonist. The hydrophilic properties of this tracer allow greater binding to surface receptors over internalized receptors. [^{11}C]-CGP-12177 has favorable characteristics for cardiac imaging, such as rapid blood clearance, high binding affinity for β_1 (k_d= 0.3 nM) and β_2 (k_d= 0.9 nM) [30, 31] receptors, and high cardiac specific binding (80–90%) [31, 32]. In addition, quantitative graphical methods that avoid the need for blood sampling have been developed for clinical applications that show good agreement with multi-injection, metabolite-corrected protocols [32, 33]. However, initial widespread clinical application of this tracer was precluded by complicated synthesis using a [^{11}C]-phosgene and low specific activities. However, recent advances in [^{11}C]-phosgene generation led to higher specific activity yields and more recent applications in preclinical models and in clinical settings [34, 35].

[^{11}C]-CGP-12388 is a hydrophilic, non-selective β-antagonist that is an isopropyl analog of [^{11}C]-CGP-12177 that was developed to overcome the synthesis difficulties of [^{11}C]-CGP-12177. Blocking studies in rodents and humans indicted high cardiac specific binding [36, 37]. Elsinga et al. [37] reported high-quality cardiac images, fast plasma clearance, low plasma protein binding, and slow metabolism of the tracer following injection in humans.

Cardiac Parasympathetic Nervous System Imaging

The preganglionic efferent nerves of the PNS pass uninterrupted from the medulla oblongata to the heart by way of the two vagal nerves. The vagal cholinergic nerves synapse with postganglionic efferent nerves in the inferior ganglia or in the basally located cardiac plexus. PNS nerve fibers mainly innervate the atria and conduction nodules and, thus, have more of an effect on chronotropy than on myocardial inotropy [1, 2].

PNS nerve conduction is mediated by the release of acetylcholine (ACh) from postganglionic terminal nerve endings. The terminal nerve ending varicosities store ACh in high concentrations in transmitter vesicles until release. Following an action potential and nerve depolarization, the varicosities empty their contents of ACh into the synaptic space for subsequent binding to muscarinic (MR) and nicotinic ACh receptors (nAChRs) [1, 2]. The predominant ACh receptor found in the heart is the G_i protein-coupled M_2 MR, which is found on cardiomyocytes and intracardiac ganglia [38]. Stimulation of this receptor decreases heart rate and reduces the force of contraction of cardiomyocytes, especially in the atria [1]. nAChRs are present in the myocardium and on nerve fibers that innervate the blood vessels, but the precise function of these receptors in mediating PNS control of cardiac function is largely unknown. Notably, the action of ACh is transient, due to rapid degradation into choline and an acetate ion by acetylcholinesterase (AChE). Following metabolism, choline is reuptaken by the terminal nerve endings resulting in continual resynthesis of ACh (Fig. 1) [1].

Imaging of PNS cardiac innervation has proven more challenging than SNS innervation imaging due to the denser distribution of PNS terminal nerves and receptors in the thinner-walled atria compared to the ventricles, coupled with the rapid degradation of ACh by AChE. Nevertheless, successful and promising radiotracers for PNS innervation imaging have been developed and are described below.

Tracers of PNS Presynaptic Nerve Activity

AChE staining has been used to quantify and map cardiac PNS innervation [39]. Donepezil is a non-competitive, high-affinity, reversible antagonist of AChE; thus, the radiotracer, [^{11}C]-donepezil, has been used to assess AChE abundance non-invasively in the brain [40, 41]. Recently, Gjerløff et al. [42, 43••] provided evidence of the utility of [^{11}C]-donepezil as a cardiac PNS innervation imaging agent in preclinical and human studies. In these studies, [^{11}C]-donepezil had low peripheral metabolism in humans over a 60-min PET scan (>90% unchanged), and had high cardiac uptake (SUV = 7.4 ± 0.8) and slow washout kinetics over a 60-min scan [42]. Importantly, the capacity to non-invasively and absolutely quantify [^{11}C]-donepezil uptake using SUV was also determined by a near linear correlation observed between SUV and metabolite-corrected kinetic models [43••]. This tracer shows promise for cardiac PNS presynaptic terminal nerve imaging and may have screening and/or prognostic value in populations with altered cardiac PNS innervation [42].

Tracers of Postsynaptic PNS Receptors

(R,S)-N-[^{11}C]-Methyl-quinuclidin-3-yl benzilate ([^{11}C]-MQNB) is a [^{11}C]-labeled hydrophilic, highly specific, non-metabolized, non-selective antagonist of MRs, which has been applied clinically for cardiac PNS activity PET imaging [44]. Ligand-receptor mathematical models that attempt to quantify the receptor concentration and ligand affinity of cardiac MR have been developed and validated in preclinical models [45, 46] and optimized in humans [47, 48] using multiple injection protocols. As such, myocardial MR density and affinity have been assessed with [^{11}C]-MQNB using multiple injection protocols in disease states known to be associated with altered cardiac autonomic nervous system balance (see below).

2-[^{18}F]-F-A-85380, a fluorine-radiolabeled analog of A-85380, a highly selective agonist of the ($\alpha_4\beta_2$ nAChR, has recently been applied to cardiovascular imaging [49]. Initial studies showed the feasibility of imaging cardiac nAChRs with 2-[^{18}F]-F-A-85380, showing good target-to-background (heart-to-lung) activity ratios on whole body PET scans in healthy volunteers and in patients with neurodegenerative disease [49]. In these studies, there were no reported differences in activity ratios between patients and controls; however, these studies did not attempt kinetic modeling and thus do not preclude the possible identification of receptor density and ligand affinity differences with refined injection protocols and kinetic modeling.

Clinical Applications/Efficacy of Autonomic PET Imaging

The ANS plays an integral role in normal cardiovascular function and disease. The ability to non-invasively assess the ANS, specifically the SNS, with nuclear imaging modalities (SPECT and PET) has proved experimentally and clinically valuable in understanding the pathophysiology and prognosis of many cardiovascular diseases [50, 51••]. As discussed above, PET imaging offers clear benefits over SPECT, and recent advances have been made in the application of PET ANS imaging in a variety of relevant cardiovascular clinical conditions. A summary of these advances is discussed below.

Evaluation of Innervation After Cardiac Transplantation

Cardiac transplantation leads to SNS denervation due to surgical transection of innervating postganglionic nerves at the base of the heart. Indeed, denervation leads to altered SNS cardiac responsiveness, contributing to exercise intolerance and altered coronary blood flow regulation to stress [52, 53]. Since all aspects of the uptake-1 mechanism (e.g., uptake, storage, metabolism) are disturbed following transplant surgery, investigators have used transplant patients to evaluate the specificity of presynaptic SNS PET tracers to each of these mechanisms early after surgery. As such, the specificity of [^{11}C]-HED, [^{11}C]-EPI, and [^{11}C]-PHEN for NE uptake, storage, and metabolism, respectively, has been evaluated and confirmed by this model [14, 18, 21•]. Recently, Bravo et al. [21•] evaluated posttransplant reinnervation at the subcellular level by simultaneously assessing the uptake index of these three tracers in transplant patients and normal controls. These investigators showed that [^{11}C]-PHEN wash greatly influenced by the overlap area of [^{11}C]-HED and [^{11}C]-EPI,

suggesting that [^{11}C]-PHEN metabolism to MAO is largely dependent on intact uptake and vesicular storage, as originally suggested by Raffel et al. in seminal [^{11}C]-PHEN studies [22].

PET imaging with [^{11}C]-HED has been extensively used to non-invasively characterize cardiac denervation and reinnervation process, and the cardiac physiological responses to reinnervation [52–54]. Initial cross-sectional studies using PET [^{11}C]-HED showed regional heterogeneity in the reinnervation process that occurred predominately in the LAD vascular perfusion territory [55]. Longitudinal studies using [^{11}C]-HED confirmed these findings and reported a reinnervation pattern that initially occurs in the anteroseptal wall in a basal to distal fashion, followed by lateral wall reinnervation, and lastly inferior wall and apical reinnervation [54]. However, the heart does not become fully reinnervated over time and some patients remain denervated late after surgery (15 years). Follow-up studies indicated that although time is a determinant of reinnervation, the likelihood of innervation is also dependent on donor and recipient age, duration and complexity of surgery [56], and diabetic status [57]. Perhaps most importantly, [^{11}C]-HED has been used to assess the significance of SNS innervation on cardiac function. It has been reported that areas of denervation have increased basal glucose metabolism compared to reinnervated areas, despite having normal oxidative capacity and normal basal coronary flow [58]. In addition, using cold pressor testing as a SNS stimulus, Di Carli et al. [52] reported decreased myocardial blood flow (MBF) in the same territories as decreased [^{11}C]-HED uptake in transplant patients, while showing that MBF was appropriately increased in areas of higher [^{11}C]-HED uptake. Along these lines, it has been shown that areas of reinnervation after transplantation have appropriate increases in chronotropy and inotropy in response to aerobic exercise, while areas of denervation have blunted responses [53].

Studies evaluating postsynaptic SNS and PNS receptor density in transplant patients with PET are lacking. A small study of early postoperative (mean 4.7±2.3 months) transplant patients showed no difference in MR binding affinity, nor MR density compared to age-matched, healthy controls when assessed with PET and [^{11}C]-MQNB [48]. Unlike SNS denervation with transplant surgery, the postganglionic nerves remain intact and may explain these findings.

Alterations in Autonomic Function with Myocardial Ischemia and Infarction

Autonomic system innervation and function is altered following an acute myocardial infarction (AMI). Seminal preclinical studies in canines showed that permanent LAD occlusion led to sympathetic denervation in the infarct area and adjacent border zone [59]. Recent, multi-tracer preclinical studies have extended these findings in vivo with PET imaging and observed that [^{11}C]-HED uptake was reduced to a similar extent as flow following an AMI, while defects relating to vesicular storage ([^{11}C]-EPI) and neurotransmitter degradation ([^{11}C]-PHEN) exceeded the perfusion defect [60] (Fig. 3). These results indicate that sympathetic dysinnervation may be apparent in the infarct border zone, rather than overt denervation present in the infarct area. On the other hand, early clinical studies have reported that the defect size corresponding to abnormal [^{11}C]-HED uptake is more extensive than perfusion defects following an AMI [61]. These studies also

showed that decrements in [^{11}C]-HED uptake were especially evident in patients with non-Q wave infarctions and were irreversible at short-term follow-up. Some studies using [^{11}C]-HED [62] have corroborated the irreversibility of post-infarct denervation, although studies with [^{18}F]-6F-DA have not [63].

β-Adrenergic receptor density (B_{max}), measured with PET and [^{11}C]-CGP-12177, has been shown to be globally reduced in the LV of patients following an AMI compared to normal controls [64–66]. More importantly, the reduction in β-adrenergic receptor density in the remote, non-infarcted zone is predictive of LV remodeling [66] and is associated with impaired systolic function prior to development of overt HF [64]. Although altered cardiac vagal activity has been suggested to have a role in post-infarct arrhythmogenesis, there is a paucity of data on in vivo PET imaging of the PNS in post-infarct patients. One study to date has assessed MR density with [^{11}C]-MQNB PET imaging in post-infarct patients using a modified two-injection protocol [67]. Mazzadi et al. [67] reported that MR density was significantly upregulated in the remote and border zone compared to the infarct zone and normal regions in healthy controls, while MR density in the infarct zone was not significantly reduced compared to normal control regions. Interestingly, the mean B_{max} per patient in the remote zone was negatively associated with resting heart rate. Importantly, elevated resting heart rate has been correlated with increased cardiovascular and all-cause mortality in healthy controls and in patients with CAD [68].

Neuronal uptake of NE is an energy-dependent process that requires oxygen for proper function. As such, the uptake-1 mechanism is impaired during ischemia and has been found to be more sensitive to a lack of oxygen than the myocardium [69]. In accordance with this hypothesis, successful reperfusion therapies that restore flow to hibernating myocardium and lead to improvements in regional and global function often fail to improve function of the SNS as characterized by large residual [^{11}C]-HED defects [70]. In line with preclinical findings, patients with multi-vessel disease and prior revascularization, but without a history of MI, show significant impairments in [^{11}C]-HED uptake compared to normal controls, despite having normal resting MBF [71]. Furthermore, there have been reports of reduced [^{11}C]-HED uptake in a similar pattern to stress-flow defects in patients with CAD, but with viable myocardium [62].

Autonomic Dysfunction with Cardiomyopathy and Heart Failure

Excessive cardiac SNS activation is a hallmark of progressive heart failure [72–74]. A compensatory increase in adrenergic drive causes desensitization/downregulation of the uptake-1 mechanism due to excess NE in the synaptic cleft. The down-regulation of uptake-1 exposes the heart and postsynaptic adrenergic receptors to greater concentrations of NE, which in turn causes desensitization/downregulation of β-adrenergic receptors, cardiac remodeling, and worsening of HF and prognosis [72]. Non-invasive, in vivo assessment of sympathetic innervation and β-adrenergic receptor density with PET imaging has helped to confirm most of these hypotheses in vivo and has clarified slightly different SNS pre- and postsynaptic functions depending on the etiology of HF.

The relationship between reduced global and focal uptake-1 in HF and cardiomyopathies has been extensively studied using [^{11}C]-HED. Accumulating evidence suggests that global [^{11}C]-HED RI is reduced in patients with both non-ischemic and ischemic HF with reduced ejection fraction (HFrEF) [75–78], in patients with HF with preserved ejection fraction (HFpEF) [79••], and in patients with hypertrophic cardiomyopathy with normal LV function [80] compared to age-matched, normal controls. In most of these studies, patients with reduced [^{11}C]-HED RI also tend to have greater heterogeneity in [^{11}C]-HED uptake between different myocardial segments. More importantly, lower global [^{11}C]-HED RI is associated with HF severity and cardiac function in patients with HFrEF [76]. In addition, lower [^{11}C]-HED is predictive of worse cardiovascular prognosis and all-cause mortality in patients with HFrEF [81, 82]. The prognostic value of [^{11}C]-HED in HFpEF has yet to be studied, but global and heterogeneous uptake of [^{11}C]-HED has recently been shown to be associated with the severity of diastolic dysfunction in HFpEF patients [79••] (Fig. 4).

The relationship between HF and cardiomyopathies and β-adrenergic receptor PET imaging is less clear and depends on the etiology of disease. In non-ischemic cardiomyopathies, investigators have reported significant decreases in β-adrenergic receptor density (B_{max}) measured with [^{11}C]-CGP-12177 [83, 84] and [^{11}C]-CGP-12388 [85] compared to age-matched controls. Tsukamoto et al. [83] showed that the reduction in [^{11}C]-CGP-12177 B_{max} occurs concomitantly with an increased ^{123}I-mIBG H/M washout, a non-invasive assessment of presynaptic nerve activity. Thus, lending credence to the supposition that β-adrenergic receptor downregulation is due to heightened SNS presynaptic nerve activity. Along these lines, Schäfers et al. [80] showed a decrease in global [^{11}C]-HED by 53% and [^{11}C]-CGP-12177 B_{max} by 28% in patients with hypertrophic cardiomyopathy (HCM) and normal EF compared to healthy controls. On the other hand, Caldwell et al. [78] did not report a significant global or regional decrease in [^{11}C]-CGP-12177 B_{max} in the non-infarct zone of patients with ischemic HF, despite these patients having significantly depressed global and regional [^{11}C]-HED PS_{nt} (uptake). However, when examining these findings together, the ischemic HF patients had significant global and regional mismatch between β-adrenergic receptor density and presynaptic innervation (B_{max}/PS_{nt}) when compared to controls. In addition, the degree of mismatch in HF patients portended a worse CV prognosis, albeit in a small group of patients. Unfortunately, the significance of the mismatch ratio has not yet been studied on a larger scale.

The PNS also plays a role in the pathophysiology of HF, but the role of PET PNS targeted imaging is far less documented than the role of the SNS. Evidence suggests that HF is associated with attenuated PNS tone and heightened β-adrenergic antagonism following muscarinic stimulation [4]. Along these lines, the density and affinity of MRs was assessed with PET and [^{11}C]-MQNB in patients with HFrEF with idiopathic dilated cardio-myopathy and healthy controls [86]. Although the binding affinity of MRs was not different between the groups, the receptor concentration (B_{max}) was significantly higher (~26%) in HF patients compared to healthy controls. In addition, MR B_{max} was negatively correlated with maximal heart rate in the patients, and injection of cold MQNB compound (0.6 mg) had less of an chronotropic effect in the patients compared to controls [86]. The authors speculate that upregulation of MR in HF may indicate a compensatory mechanism to counterbalance

excessive β-adrenergic receptor stimulation. Further study is needed to confirm this theory and to assess the role of PNS imaging in other HF etiologies.

Role of PET SNS Imaging in Cardiac Resynchronization Therapy

Cardiac resynchronization therapy (CRT) is a potential treatment option for patients with HF, particularly in those with an LVEF <35%, a wide QRS complex (≥150 ms), and a New York Heart Association (NYHA) class of II–IV [87]. CRT has been shown to improve HF symptoms and reduce hospitalizations and life-threatening arrhythmias in some patients [87]. However, about one-third of patients receiving CRT do not respond to therapy [88]. Although it is not fully elucidated, some evidence suggests that modulation of the neurohumoral environment plays a role in improved LV function with CRT [89]. Recently, PET SNS imaging with [^{11}C]-HED has been used to investigate the role of cardiac innervation in CRT [90••, 91]. In a small study (n= 10), patients with dilated cardiomyopathy and moderate severity HF (LVEF ≤35%; NHYA II–III) underwent [^{11}C]-HED PET imaging prior to and early (1 week and 3 months) after CRT implantation [90••]. Patients that responded to CRT therapy (reduction in LVESV of ≥15% at the 3-month follow-up) had higher [^{11}C]-HED SUVs and less regional heterogeneity in tracer uptake at baseline compared to non-responders. In addition, responders had significant improvements in total myocardial [^{11}C]-HED SUV and regional heterogeneity compared to non-responders. In partial agreement, another study of similar design showed that regional heterogeneity, but not global myocardial [^{11}C]-HED uptake (SUV), improved 3 months after CRT implantation in moderate to severe (NHYA III–IV) HF patients [91]. In contrast to the above, only impaired myocardial segments (<76% uptake of maximum) at baseline improved following CRT in this study [91]. This study did not distinguish improvements between responders and non-responders to CRT. Together, these studies support an improvement in SNS presynaptic function with CRT and provide some evidence that [^{11}C]-HED PET imaging may help to select patients for CRT. Indeed, larger scale studies are needed to determine the screening potential of [^{11}C]-HED PET imaging for selection of patients who may benefit from CRT.

Predicting Ventricular Arrhythmias and Sudden Cardiac Death with ANS Imaging

Currently, reduced LVEF ≤35% is the only criterion for eligibility of implantable cardioverter defibrillator (ICD) therapy for primary prevention of sudden cardiac death (SCD) [92]. However, only a small fraction of patients with depressed LVEF develop SCD [93]. Impaired sympathetic innervation and pre/postsynaptic balance is believed to cause electromechanical instability leading to the development of ventricular arrhythmogenesis [78, 94]. Accumulating evidence in preclinical and clinical studies suggest a critical role of sympathetic cardiac PET imaging in predicting lethal cardiac arrhythmias and SCD [51••, 95]. The results of key studies in elucidating this relationship are summarized below.

Initial preclinical studies showed that pigs susceptible to inducible ventricular tachycardia (VT) following an AMI had larger innervation/perfusion ([^{11}C]-EPI/[^{13}N]-ammonia) mismatch areas in the infarct border zone compared to pigs that did not have inducible VT

[60]. Interestingly, there were no differences in denervation area measured with PET [^{11}C]-HED between inducible and non-inducible pigs. Electrophysiological studies (EPS) by the same group also showed that the innervation/perfusion mismatch ratio was strongly associated with reduced myocardial voltage and the site of earliest VT activation in pigs following an AMI [95].

In contrast to preclinical studies, clinical studies have shown that the total denervation area assessed with PET [^{11}C]-HED was more important in predicting ventricular arrhythmias (VA) [51••, 96] and SCD [51••] than the innervation/perfusion mismatch area and the area of denervated but viable myocardium. In the PAREPET (Prediction of Arrhythmic Events with Positron Emission Tomography) study, a relatively larger group of patients (n = 204) with ischemic cardiomyopathy that were eligible to receive a primary prevention ICD (LVEF <35%) underwent complementary PET imaging of resting flow ([^{13}N]-ammonia), myocardial viability (insulin-stimulated ([^{18}F]-FDG), and sympathetic innervation ([^{11}C]-HED) at baseline [51••]. The primary end-point in this study was SCD defined as arrhythmic death or discharge due to VT/VF (fibrillation) >240 beats per minute. At baseline, patients had a significantly larger denervation volume (27 ±11% of the LV) compared to infarct volume (20 ±9% of the LV), with 8 ±6% of the myocardium being denervated but viable. PET quantification of resting flow, viability, and denervation for two representative subjects from this study is shown in Fig. 5. During an average follow-up of 4.1 years, the subjects that developed SCD had significantly larger volumes of total denervated myocardium and viable denervated myocardium compared to subjects without SCD, where infarct volume, hibernating myocardium, LVEF, and LV mass were not different. The total volume of denervated and viable denervated myocardium predicted time to SCD. Multi-variate analysis revealed that only denervated myocardial volume independently predicted time to SCD.

Further studies have confirmed the importance of total denervated myocardium volume in predicting VA in patients with ischemic cardiomyopathy and reduced systolic function [96]. In a similar patient demographic as PAREPET, patients with newly placed ICDs and inducible VA during an EPS had larger denervation areas as assessed with [^{11}C]-HED compared to non-inducible patients. In addition, there were no differences in the innervation/perfusion mismatch ratio in patients with and without inducible VA. In contrast to the PAREPET study, denervation volume did not remain an independent predictor of inducible VA in multi-variate analysis. Nonetheless, these studies indicate that global denervation size may be more important in predicting VA and SCD than regional denervation. In addition, these studies indicate that PET imaging of sympathetic neurons with [^{11}C]-HED may help to risk stratify patients that would benefit from ICD therapy. Future larger scale trials are needed to confirm these results in patients with and without reduced EF.

Conclusions

Many ANS radioligands have been synthesized for PET cardiac imaging, but to date, the most clinically relevant PET tracer has been [^{11}C]-HED. Accumulating evidence have indicated the utility of [^{11}C]-HED in relevant clinical issues, such as predicting lethal arrhythmias, SCD, and all-cause mortality in HFrEF patients. More recent investigators have provided some evidence of the utility of [^{11}C]-HED in more elusive cardiovascular clinical

conditions, such as in HFpEF and in predicting response to CRT in eligible patients. Tracers that target β-adrenergic receptor density have also shown some value, especially in regard to LV remodeling and systolic dysfunction following an AMI. Conversely, tracers that target cardiac PNS innervation have been less successful for cardiac ANS PET imaging, but recent investigations point to the potential utility of novel tracers, such as [^{11}C]-donepezil, in this arena. The future application of [^{11}C]-HED and newly designed ^{18}F-labeled tracers for targeting the ANS hold promise for the evaluation and management of a wide range of cardiovascular diseases, including the prognostication of patients with HFpEF.

References

Papers of particular interest, published recently, have been highlighted as:

• Of importance

•• Of major importance

1. Hall, JE. Guyton and Hall textbook of medical physiology. 13. Philadelphia, PA: Saunders Elsevier; 2015. Chapter 60: The autonomic nervous system and the adrenal medulla; p. 748-760.
2. Battipaglia, I., Lanza, GA. Autonomic Innervation of the Heart. New York City: Springer Publishing; 2015. Chapter 1: The Autonomic Nervous System of the Heart; p. 1-12.
3. Merz CNB, Elboudwarej O, Mehta P. The autonomic nervous system and cardiovascular health and disease: a complex balancing act. JACC. 2015; 3:383–5. [PubMed: 25951758]
4. Olshansky B, Sabbah HN, Hauptman PJ, Colucci WS. Parasympathetic nervous system and heart failure pathophysiology and potential implications for therapy. Circulation. 2008; 118:863–71. [PubMed: 18711023]
5. Malpas SC. Sympathetic nervous system overactivity and its role in the development of cardiovascular disease. Physiol Rev. 2010; 90:513–57. [PubMed: 20393193]
6. Esler M, Kaye D. Sympathetic nervous system activation in essential hypertension, cardiac failure and psychosomatic heart disease. J Cardiovasc Pharmacol. 2000; 35:S1–7.
7. Barron HV, Lesh MD. Autonomic nervous system and sudden cardiac death. J Am Coll Cardiol. 1996; 27:1053–60. [PubMed: 8609321]
8. Travin MI. Clinical applications of myocardial innervation imaging. Cardiol Clin. 2016; 34:133–47. [PubMed: 26590785]
9. Higuchi T, Schwaiger M. Imaging cardiac neuronal function and dysfunction. Curr Cardiol Rep. 2006; 8:131–8. [PubMed: 16524540]
10. Henneman MM, Bengel FM, van der Wall EE, Knuuti J, Bax JJ. Cardiac neuronal imaging: application in the evaluation of cardiac disease. J Nucl Cardiol. 2008; 15:442–55. [PubMed: 18513651]
11. Slart, RH., van der Meer, P., Tio, RA., van Veldhuisen, DJ., Elsinga, PH. Autonomic Innervation of the Heart. New York City: Springer Publishing; 2015. Chapter 11: PET imaging of myocardial β-adrenoceptors; p. 235-253.
12•. Raffel DM, Chen W, Jung Y-W, Jang KS, Gu G, Cozzi NV. Radiotracers for cardiac sympathetic innervation: transport kinetics and binding affinities for the human norepinephrine transporter. Nucl Med Biol. 2013; 40:331–7. This study provides a thorough comparison of the kinetics and binding affinities of novel and established SNS presynaptic PET radiotracers for the human norepinephrine transporter. [PubMed: 23306137]
13. Tipre DN, Fox JJ, Holt DP, et al. In vivo PET imaging of cardiac presynaptic sympathoneuronal mechanisms in the rat. J Nucl Med. 2008; 49:1189–95. [PubMed: 18552143]
14. Münch G, Nguyen NT, Nekolla S, et al. Evaluation of sympathetic nerve terminals with [11C] epinephrine and [11C] hydroxyephedrine and positron emission tomography. Circulation. 2000; 101:516–23. [PubMed: 10662749]

15. Raffel DM, Chen W. Binding of [3H] mazindol to cardiac norepinephrine transporters: kinetic and equilibrium studies. Naunyn Schmiedeberg's Arch Pharmacol. 2004; 370:9–16. [PubMed: 15300361]

16. Rosenspire KC, Haka MS, Van Dort ME, et al. Synthesis and preliminary evaluation of carbon-11-meta-hydroxyephedrine: a false transmitter agent for heart neuronal imaging. J Nucl Med. 1990; 31:1328–34. [PubMed: 2384800]

17. Law MP, Osman S, Davenport RJ, Cunningham VJ, Pike VW, Camici PG. Biodistribution and metabolism of [N-methyl-11C]-m-hydroxyphedrine in the rat. Nucl Med Biol. 1997; 24:417–24. [PubMed: 9290077]

18. Schwaiger M, Kalff V, Rosenspire K, et al. Noninvasive evaluation of sympathetic nervous system in human heart by positron emission tomography. Circulation. 1990; 82:457–64. [PubMed: 2372893]

19. Thackeray JT, Beanlands RS, DaSilva JN. Presence of specific 11C-meta-hydroxyephedrine retention in heart, lung, pancreas, and brown adipose tissue. J Nucl Med. 2007; 48:1733–40. [PubMed: 17873125]

20. Nguyen NT, DeGrado TR, Chakraborty P, Wieland DM, Schwaiger M. Myocardial kinetics of carbon-11-epinephrine in the isolated working rat heart. J Nucl Med. 1997; 38:780. [PubMed: 9170446]

21•. Bravo PE, Lautamäki R, Carter D, et al. Mechanistic insights into sympathetic neuronal regeneration: multitracer molecular imaging of catecholamine handling after cardiac transplantation. Circulation: Cardiovascular Imaging. 2015; 8:e003507. This is the first-in-human study that assessed ^{11}C-hydroxyephedrine, ^{11}C-epinephrine, and ^{11}C-phenylephrine simultaneously with myocardial blood flow (^{13}N-ammonia) in heart transplant patients and healthy controls. As such, this study was able to provide mechanistic information on the regrowth of SNS neurons post transplant. [PubMed: 26245765]

22. Raffel DM, Corbett JR, del Rosario RB, Mukhopadhyay SK. Sensitivity of [11C] phenylephrine kinetics to monoamine oxidase activity in normal human heart. J Nucl Med. 1999; 40:232. [PubMed: 10025828]

23. Del, Rosario RB., Jung, Y-W., Caraher, J., Chakraborty, PK., Wieland, DM. Synthesis and preliminary evaluation of [11 C]-(−)-phenylepnrine as a functional heart neuronal PET agent. Nucl Med Biol. 1996; 23:611–6. [PubMed: 8905825]

24. Chirakal R, Coates G, Firnau G, Schrobilgen GJ, Nahmias C. Direct radiofluorination of dopamine: 18 F-labeled 6-fluorodopamine for imaging cardiac sympathetic innervation in humans using positron emission tomography. Nucl Med Biol. 1996; 23:41–5. [PubMed: 9004913]

25. Goldstein D, Holmes C, Stuhlmuller JE, Lenders JW, Kopin IJ. 6-[18F] Fluorodopamine positron emission tomographic scanning in the assessment of cardiac sympathoneural function—tudies in normal humans. Clin Auton Res. 1997; 7:17–29. [PubMed: 9074825]

26. Yu M, Bozek J, Lamoy M, et al. Evaluation of LMI1195, a novel 18F-labeled cardiac neuronal PET imaging agent, in cells and animal models. Circ Cardiovasc Imaging. 2011; 4:435–43. [PubMed: 21555377]

27. Werner RA, Rischpler C, Onthank D, et al. Retention kinetics of the 18F-labeled sympathetic nerve PET tracer LMI1195: comparison with 11C-Hydroxyephedrine and 123I-MIBG. J Nucl Med. 2015; 56:1429–33. [PubMed: 26182969]

28. Higuchi T, Yousefi BH, Reder S, et al. Myocardial kinetics of a novel [F]-labeled sympathetic nerve PET tracer LMI1195 in the isolated perfused rabbit heart. J Am Coll Cardiol Img. 2015; 8:1229–31.

29••. Sinusas AJ, Lazewatsky J, Brunetti J, et al. Biodistribution and radiation dosimetry of LMI1195: first-in-human study of a novel 18F-labeled tracer for imaging myocardial innervation. J Nucl Med. 2014; 55:1445–51. This was the first-in-human study to assess the biodistribution and radiation dosimetry of F-LMI1195, an ^{18}F-analog of the widely used SPECT tracer, ^{123}I-meta-iodobenzylguanidine (mIBG). This study showed acceptable radiation dosimetry and very favorable target-to-background ratio for cardiac imaging. [PubMed: 24994931]

30. Mohell N, Dicker A. The β-adrenergic radioligand [3H] CGP-12177, generally classified as an antagonist, is a thermogenic agonist in brown adipose tissue. Biochem J. 1989; 261:401–5. [PubMed: 2570569]

31. Van Waarde A, Meeder JG, Blanksma PK, et al. Uptake of radioligands by rat heart and lung in vivo: CGP 12177 does and CGP 26505 does not reflect binding to β-adrenoceptors. Eur J Pharmacol. 1992; 222:107–12. [PubMed: 1361437]
32. Delforge J, Syrota A, Lancon JP, et al. Cardiac beta-adrenergic receptor density measured in vivo using PET, CGP 12177, and a new graphical method. J Nucl Med. 1991; 32:739–48. [PubMed: 1672889]
33. Delforge J, Mesangeau D, Dolle F, et al. In vivo quantification and parametric images of the cardiac β-adrenergic receptor density. J Nucl Med. 2002; 43:215–26. [PubMed: 11850488]
34. K-i N, Kuge Y, K-i S, et al. A simplified and improved synthesis of [11C] phosgene with iron and iron (III) oxide. Nucl Med Biol. 2002; 29:345–50. [PubMed: 11929705]
35. Nishijima K, Kuge Y, Seki K, et al. Preparation and pharmaceutical evaluation for clinical application of high specific activity S-(−)[11C] CGP-12177, a radioligand for β-adrenoreceptors. Nucl Med Commun. 2004; 25:845–9. [PubMed: 15266181]
36. Momose M, Reder S, Raffel DM, et al. Evaluation of cardiac β-adrenoreceptors in the isolated perfused rat heart using (S)-11C-CGP12388. J Nucl Med. 2004; 45:471–7. [PubMed: 15001690]
37. Elsinga PH, Doze P, van Waarde A, et al. Imaging of β-adrenoceptors in the human thorax using (S)-[11 C] CGP12388 and positron emission tomography. Eur J Pharmacol. 2001; 433:173–6. [PubMed: 11755150]
38. Dhein S, van Koppen CJ, Brodde OE. Muscarinic receptors in the mammalian heart. Pharmacol Res. 2001; 44:161–82. [PubMed: 11529684]
39. Pauza DH, Saburkina I, Rysevaite K, et al. Neuroanatomy of the murine cardiac conduction system: a combined stereomicroscopic and fluorescence immunohistochemical study. Auton Neurosci. 2013; 176:32–47. [PubMed: 23403121]
40. Okamura N, Funaki Y, Tashiro M, et al. In vivo visualization of donepezil binding in the brain of patients with Alzheimer's disease. Br J Clin Pharmacol. 2008; 65:472–9. [PubMed: 18070217]
41. Hiraoka K, Okamura N, Funaki Y, et al. Cholinergic deficit and response to donepezil therapy in Parkinson's disease with dementia. Eur Neurol. 2012; 68:137–43. [PubMed: 22832236]
42. Gjerløff T, Fedorova T, Knudsen K, et al. Imaging acetylcholinesterase density in peripheral organs in Parkinson's disease with 11C-donepezil PET. Brain. 2014:awu369.
43••. Gjerløff T, Jakobsen S, Nahimi A, et al. In vivo imaging of human acetylcholinesterase density in peripheral organs using 11C-donepezil: dosimetry, biodistribution, and kinetic analyses. J Nucl Med. 2014; 55:1818–24. This was the first-in-human study to assess the biodistribution and radiation dosimetry of ^{11}C-donepezil, a radiotracer that binds to acetylcholinesterase, in peripheral organs including the heart and liver. Cardiac PNS presynaptic imaging has been unsuccessful to date. This study provides promising data for future cardiac PNS presynaptic imaging, including high cardiac specific binding, high cardiac uptake, and the ability to accurately quantify cardiac images without arterial blood sampling and complex modeling. [PubMed: 25324520]
44. Le Guludec, D., Delforge, J., Dollé, F. Autonomic Innervation of the Heart. New York City: Springer Publishing; 2015. Chapter 6: Imaging the parasympathetic cardiac innervation with PET; p. 111-135.
45. Delforge J, Janier M, Syrota A, et al. Noninvasive quantification of muscarinic receptors in vivo with positron emission tomography in the dog heart. Circulation. 1990; 82:1494–504. [PubMed: 2401078]
46. Delforge J, Syrota A, Mazoyer B. Identifiability analysis and parameter identification of an in vivo ligand-receptor model from PET data. IEEE Trans Biomed Eng. 1990; 37:653–61. [PubMed: 2394453]
47. Delforge J, Le Guludec D, Syrota A, et al. Quantification of myocardial muscarinic receptors with PET in humans. J Nucl Med. 1993; 34:981–91. [PubMed: 8509869]
48. Le Guludec D, Delforge J, Syrota A, et al. In vivo quantification of myocardial muscarinic receptors in heart transplant patients. Circulation. 1994; 90:172–8. [PubMed: 8025993]
49. Bucerius J, Joe AY, Schmaljohann J, et al. Feasibility of 2–deoxy–2–[18F] fluoro–D–glucose–A85380–PET for imaging of human cardiac nicotinic acetylcholine receptors in vivo. Clin Res Cardiol. 2006; 95:105–9. [PubMed: 16598519]

50. Jacobson AF, Senior R, Cerqueira MD, et al. Myocardial iodine-123 meta-iodobenzylguanidine imaging and cardiac events in heart failure: results of the prospective ADMIRE-HF (AdreView Myocardial Imaging for Risk Evaluation in Heart Failure) study. J Am Coll Cardiol. 2010; 55:2212–21. [PubMed: 20188504]

51••. Fallavollita JA, Heavey BM, Luisi AJ Jr, et al. Regional myocardial sympathetic denervation predicts the risk of sudden cardiac arrest in ischemic cardiomyopathy. J Am Coll Cardiol. 2014; 63:141–9. This is the first study showing the prognostic value of ^{11}C-hydroxyephdrine in predicting time to sudden cardiac arrest in patients with ischemic cardiomyopathy and reduced left ventricular ejection fraction. [PubMed: 24076296]

52. Di, Carli MF., Tobes, MC., Mangner, T., et al. Effects of cardiac sympathetic innervation on coronary blood flow. N Engl J Med. 1997; 336:1208–16. [PubMed: 9110908]

53. Bengel FM, Ueberfuhr P, Schiepel N, Nekolla SG, Reichart B, Schwaiger M. Effect of sympathetic reinnervation on cardiac performance after heart transplantation. N Engl J Med. 2001; 345:731–8. [PubMed: 11547742]

54. Bengel FM, Ueberfuhr P, Ziegler SI, Nekolla S, Reichart B, Schwaiger M. Serial assessment of sympathetic reinnervation after orthotopic heart transplantation. A longitudinal study using PET and C-11 hydroxyephedrine. Circulation. 1999; 99:1866–71. [PubMed: 10199884]

55. Schwaiger M, Hutchins GD, Kalff V, et al. Evidence for regional catecholamine uptake and storage sites in the transplanted human heart by positron emission tomography. J Clin Investig. 1991; 87:1681. [PubMed: 2022739]

56. Bengel FM, Ueberfuhr P, Hesse T, et al. Clinical determinants of ventricular sympathetic reinnervation after orthotopic heart transplantation. Circulation. 2002; 106:831–5. [PubMed: 12176956]

57. Bengel FM, Ueberfuhr P, Schäfer D, Nekolla SG, Reichart B, Schwaiger M. Effect of diabetes mellitus on sympathetic neuronal regeneration studied in the model of transplant reinnervation. J Nucl Med. 2006; 47:1413–9. [PubMed: 16954547]

58. Bengel FM, Ueberfuhr P, Ziegler SI, et al. Non-invasive assessment of the effect of cardiac sympathetic innervation on metabolism of the human heart. Eur J Nucl Med. 2000; 27:1650–7. [PubMed: 11105821]

59. Barber MJ, Mueller TM, Henry DP, Felten S, Zipes DP. Transmural myocardial infarction in the dog produces sympathectomy in noninfarcted myocardium. Circulation. 1983; 67:787–96. [PubMed: 6825234]

60. Lautamaki R, Sasano T, Higuchi T, et al. Multiparametric molecular imaging provides mechanistic insights into sympathetic innervation impairment in the viable infarct border zone. J Nucl Med. 2015; 56:457–63. [PubMed: 25635137]

61. Allman KC, Wieland DM, Muzik O, Degrado TR, Wolfe ER, Schwaiger M. Carbon-11 hydroxyephedrine with positron emission tomography for serial assessment of cardiac adrenergic neuronal function after acute myocardial infarction in humans. J Am Coll Cardiol. 1993; 22:368–75. [PubMed: 8335806]

62. Fricke E, Eckert S, Dongas A, et al. Myocardial sympathetic innervation in patients with symptomatic coronary artery disease: follow-up after 1 year with neurostimulation. J Nucl Med. 2008; 49:1458–64. [PubMed: 18703600]

63. Fallen EL, Coates G, Nahmias C, et al. Recovery rates of regional sympathetic reinnervation and myocardial blood flow after acute myocardial infarction. Am Heart J. 1999; 137:863–9. [PubMed: 10220635]

64. Ohte N, Narita H, Iida A, et al. Cardiac β-adrenergic receptor density and myocardial systolic function in the remote noninfarcted region after prior myocardial infarction with left ventricular remodelling. Eur J Nucl Med Mol Imaging. 2012; 39:1246–53. [PubMed: 22588626]

65. John AS, Mongillo M, Depre C, et al. Pre-and post-synaptic sympathetic function in human hibernating myocardium. Eur J Nucl Med Mol Imaging. 2007; 34:1973–80. [PubMed: 17661029]

66. Spyrou N, Rosen SD, Fath-Ordoubadi F, et al. Myocardial beta-adrenoceptor density one month after acute myocardial infarction predicts left ventricular volumes at six months. J Am Coll Cardiol. 2002; 40:1216–24. [PubMed: 12383568]

67. Mazzadi AN, Pineau J, Costes N, et al. Muscarinic receptor upregulation in patients with myocardial infarction: a new paradigm. Circ Cardiovasc Imaging. 2009; 2:365–72. [PubMed: 19808624]
68. Fox K, Borer JS, Camm AJ, et al. Resting heart rate in cardiovascular disease. J Am Coll Cardiol. 2007; 50:823–30. [PubMed: 17719466]
69. Luisi AJ, Suzuki G, Haka MS, Toorongian SA, Canty JM, Fallavollita JA. Regional 11C-hydroxyephedrine retention in hibernating myocardium: chronic inhomogeneity of sympathetic innervation in the absence of infarction. J Nucl Med. 2005; 46:1368–74. [PubMed: 16085596]
70. Fallavollita JA, Banas MD, Suzuki G, Sajjad M, Canty JM Jr. 11C-meta-hydroxyephedrine defects persist despite functional improvement in hibernating myocardium. J Nucl Cardiol. 2010; 17:85–96. [PubMed: 19902319]
71. Bülow H, Stahl F, Lauer B, et al. Alterations of myocardial presyn-aptic sympathetic innervation in patients with multi-vessel coronary artery disease but without history of myocardial infarction. Nucl Med Commun. 2003; 24:233–9. [PubMed: 12612463]
72. Haider N, Baliga RR, Chandrashekhar Y, Narula J. Adrenergic excess, hNET1 down-regulation, and compromised mIBG uptake in heart failure: poverty in the presence of plenty. J Am Coll Cardiol Img. 2010; 3:71–5.
73. Cohn JN, Levine TB, Olivari MT, et al. Plasma norepinephrine as a guide to prognosis in patients with chronic congestive heart failure. N Engl J Med. 1984; 311:819–23. [PubMed: 6382011]
74. Kaye DM, Lambert GW, Lefkovits J, Morris M, Jennings G, Esler MD. Neurochemical evidence of cardiac sympathetic activation and increased central nervous system norepinephrine turnover in severe congestive heart failure. J Am Coll Cardiol. 1994; 23:570–8. [PubMed: 8113536]
75. Matsunari I, Aoki H, Nomura Y, et al. Iodine-123 metaiodobenzylguanidine imaging and carbon-11 hydroxyephedrine positron emission tomography compared in patients with left ventricular dysfunction. Circ Cardiovasc Imaging. 2010; 3:595–603. [PubMed: 20534790]
76. Bengel F, Permanetter B, Ungerer M, Nekolla S, Schwaiger M. Relationship between altered sympathetic innervation, oxidative metabolism and contractile function in the cardiomyopathic human heart; a non-invasive study using positron emission tomography. Eur Heart J. 2001; 22:1594–600. [PubMed: 11492989]
77. Rijnierse MT, Allaart CP, de Haan S, et al. Sympathetic denervation is associated with microvascular dysfunction in non-infarcted myocardium in patients with cardiomyopathy. Eur Heart J Cardiovasc Imaging. 2015:jev013.
78. Caldwell JH, Link JM, Levy WC, Poole JE, Stratton JR. Evidence for pre-to postsynaptic mismatch of the cardiac sympathetic nervous system in ischemic congestive heart failure. J Nucl Med. 2008; 49:234–41. [PubMed: 18199620]
79••. Aikawa T, Naya M, Tomiyama Y, et al. Impairment of myocardial sympathetic innervation and its heterogeneity are associated with diastolic dysfunction in patients with heart failure and preserved ejection fraction: C11-hydroxyephedrine PET study. J Nucl Med. 2016; 57:231. This is the first study showing that global ^{11}C-hydroxyephdrine retention index is reduced and ^{11}C-hydroxyephdrine uptake heterogeneity is increased in patients with heart failure and preserved ejection fraction (HFpEF). [PubMed: 26742708]
80. Schäfers M, Dutka D, Rhodes CG, et al. Myocardial presynaptic and postsynaptic autonomic dysfunction in hypertrophic cardiomyopathy. Circ Res. 1998; 82:57–62. [PubMed: 9440705]
81. Fujita W, Matsunari I, Aoki H, Nekolla SG, Kajinami K. Prediction of all-cause death using 11C-hydroxyephedrine positron emission tomography in Japanese patients with left ventricular dysfunction. Ann Nucl Med. 2016:1–7.
82. Pietilä M, Malminiemi K, Ukkonen H, et al. Reduced myocardial carbon-11 hydroxy ephedrine retention is associated with poor prognosis in chronic heart failure. Eur J Nucl Med. 2001; 28:373–6. [PubMed: 11315607]
83. Tsukamoto T, Morita K, Naya M, et al. Decreased myocardial β-adrenergic receptor density in relation to increased sympathetic tone in patients with nonischemic cardiomyopathy. J Nucl Med. 2007; 48:1777–82. [PubMed: 17942801]

84. Naya M, Tsukamoto T, Morita K, et al. Myocardial β-adrenergic receptor density assessed by 11C-CGP12177 PET predicts improvement of cardiac function after carvedilol treatment in patients with idiopathic dilated cardiomyopathy. J Nucl Med. 2009; 50:220–5. [PubMed: 19164238]
85. de Jong RM, Willemsen AT, Slart RH, et al. Myocardial β-adrenoceptor downregulation in idiopathic dilated cardiomyopathy measured in vivo with PET using the new radioligand (S)-[11C] CGP12388. Eur J Nucl Med Mol Imaging. 2005; 32:443–7. [PubMed: 15592928]
86. Le Guludec D, Cohen-Solal A, Delforge J, Delahaye N, Syrota A, Merlet P. Increased myocardial muscarinic receptor density in idiopathic dilated cardiomyopathy: an in vivo PET study. Circulation. 1997; 96:3416–22. [PubMed: 9396436]
87. Russo AM, Stainback RF, Bailey SR, et al. ACCF/HRS/AHA/ASE/ HFSA/SCAI/SCCT/SCMR 2013 appropriate use criteria for implantable cardioverter-defibrillators and cardiac resynchronization therapy: a report of the American College of Cardiology Foundation appropriate use criteria task force, Heart Rhythm Society, American Heart Association, American Society of Echocardiography, Heart Failure Society of America, Society for Cardiovascular Angiography and Interventions, Society of Cardiovascular Computed Tomography, and Society for Cardiovascular Magnetic Resonance. J Am Coll Cardiol. 2013; 61:1318–68. [PubMed: 23453819]
88. Daubert C, Behar N, Martins RP, Mabo P, Leclercq C. Avoiding non-responders to cardiac resynchronization therapy: a practical guide. Eur Heart J. 2016:ehw270.
89. Boriani G, Regoli F, Saporito D, et al. Neurohormones and inflammatory mediators in patients with heart failure undergoing cardiac resynchronization therapy: time courses and prediction of response. Peptides. 2006; 27:1776–86. [PubMed: 16621149]
90••. Martignani C, Diemberger I, Nanni C, et al. Cardiac resynchronization therapy and cardiac sympathetic function. Eur J Clin Invest. 2015; 45:792–9. This is the first study showing that global ^{11}C-hydroxyephdrine uptake and ^{11}C-hydroxyephdrine uptake heterogeneity may be able to predict response to cardiac resynchronization therapy in patients with heart failure and reduced left ventricular ejection fraction. [PubMed: 26036750]
91. Capitanio S, Nanni C, Marini C, et al. Heterogeneous response of cardiac sympathetic function to cardiac resynchronization therapy in heart failure documented by 11 [C]-hydroxy-ephedrine and PET/ CT. Nucl Med Biol. 2015; 42:858–63. [PubMed: 26239084]
92. Epstein AE, Dimarco JP, Ellenbogen KA, et al. ACC/AHA/HRS 2008 guidelines for Device-Based Therapy of Cardiac Rhythm Abnormalities: executive summary. Heart Rhythm. 2008; 5:934–55. [PubMed: 18534377]
93. Wellens HJ, Schwartz PJ, Lindemans FW, et al. Risk stratification for sudden cardiac death: current status and challenges for the future. Eur Heart J. 2014; 35:1642–51. [PubMed: 24801071]
94. Verrier RL, Antzelevitch C. Autonomic aspects of arrhythmogenesis: the enduring and the new. Curr Opin Cardiol. 2004; 19:2–11. [PubMed: 14688627]
95. Sasano T, Abraham MR, Chang KC, et al. Abnormal sympathetic innervation of viable myocardium and the substrate of ventricular tachycardia after myocardial infarction. J Am Coll Cardiol. 2008; 51:2266–75. [PubMed: 18534275]
96. Rijnierse MT, Allaart CP, de Haan S, et al. Non-invasive imaging to identify susceptibility for ventricular arrhythmias in ischaemic left ventricular dysfunction. Heart. 2016; 102:832–40. [PubMed: 26843532]

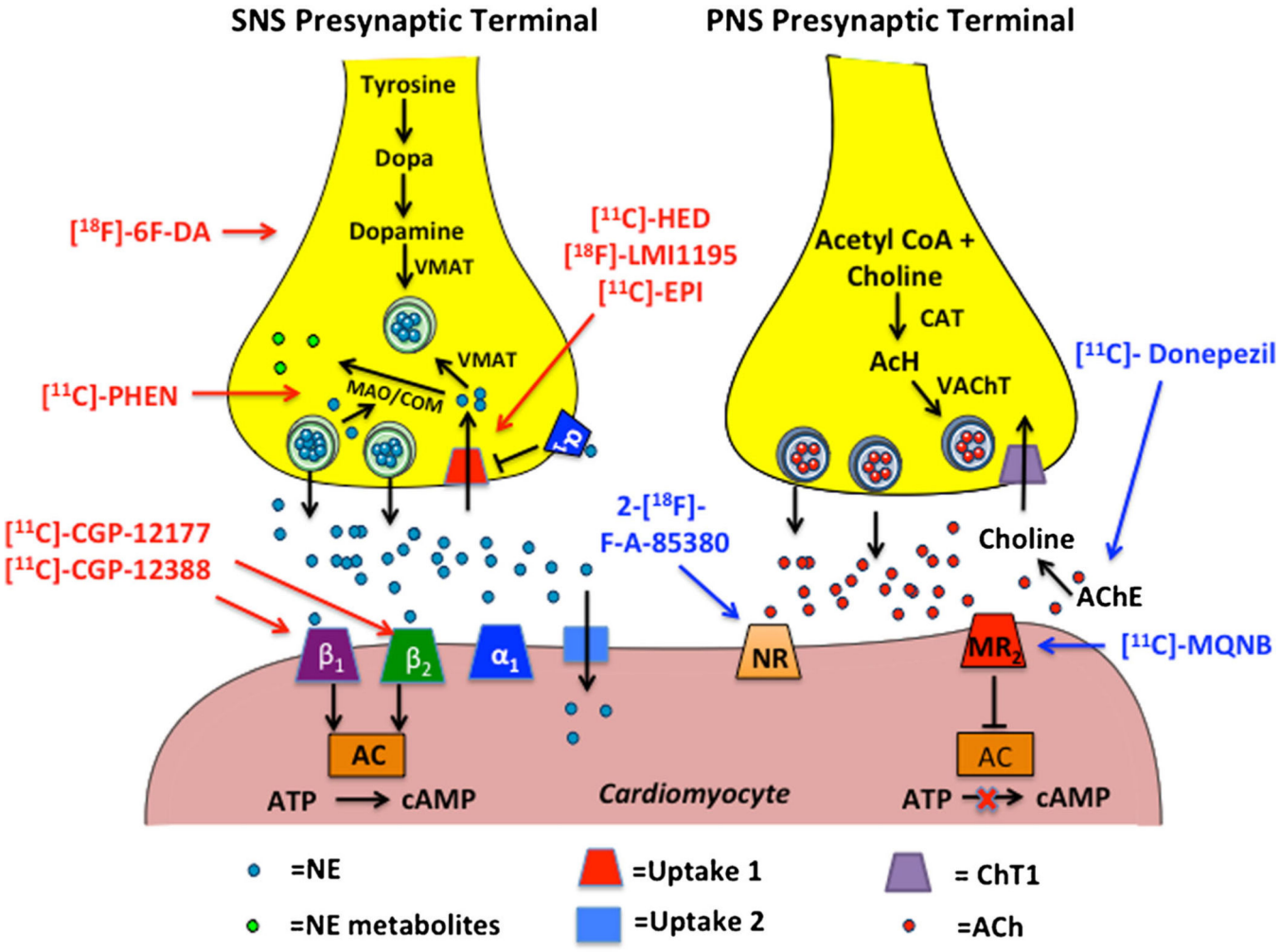

Fig. 1.

Depiction of postganglionic SNS and PNS nerve endings. *Left panel*: the synthesis and release of norepinephrine in postganglionic SNS nerve endings and subsequent binding to postsynaptic receptors on cardiomyocytes. The *tracers in red* depict SNS pre- and postsynaptic radioanalogs. *Right panel*: the synthesis and release of acetylcholine in the terminal nerve ending and varicosities of postganglionic PNS nerve endings and subsequent binding to postsynaptic receptors on cardiomyocytes. *Tracers in blue* depict PNS pre- and postsynaptic radioanalogs. *AC* adenylyl cyclase, *ACh* acetylcholine, *AChE* acetylcholinesterase, *ATP* adenosine triphosphate, *CAT* choline-acetyl-transferase, *COM* catechol-O-methyltransferase, *cAMP* cyclic adenosine monophosphate, *MAO* monoamine oxidase, MR_2 muscarinic receptor 2, *NE* norepinephrine, *NR* $\alpha_4\beta_2$ nicotinic receptor, *VMAT* vesicular monoamine transporter, ^{18}F-6F-DA 6-^{18}F-fluorodopamine, *PHEN* phenylephrine, *EPI* epinephrine, *HED* hydroxyephedrine, *MQNB* (R,S)-N-[^{11}C]-methyl-quinuclidin-3-yl benzilate

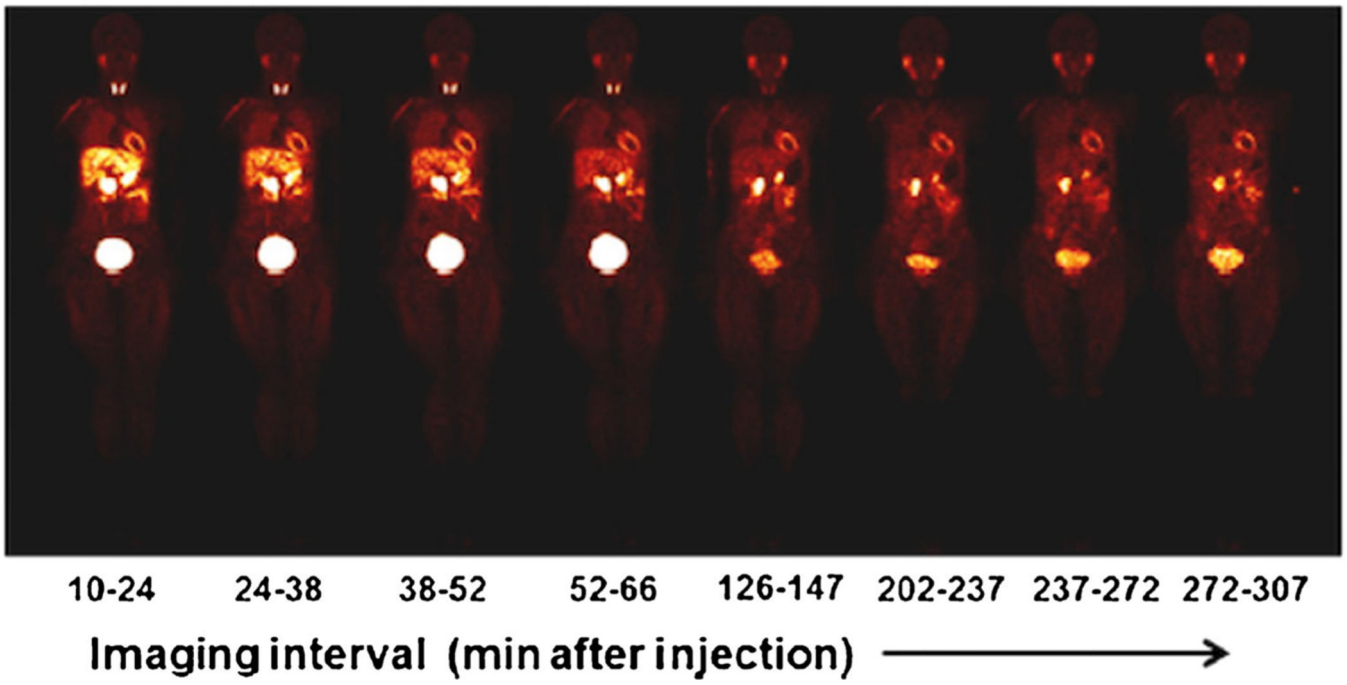

Fig. 2.

Representative series of whole body [^{18}F]-LMI1195 coronal images at mid-myocardial level in a healthy human volunteer acquired over 5 h after injection (average, 193.5 ±37.4 MBq [5.23 ±1.01 mCi]). Each whole body image is scaled to maximum value within that image (this research was originally published in *JNM* [29••])

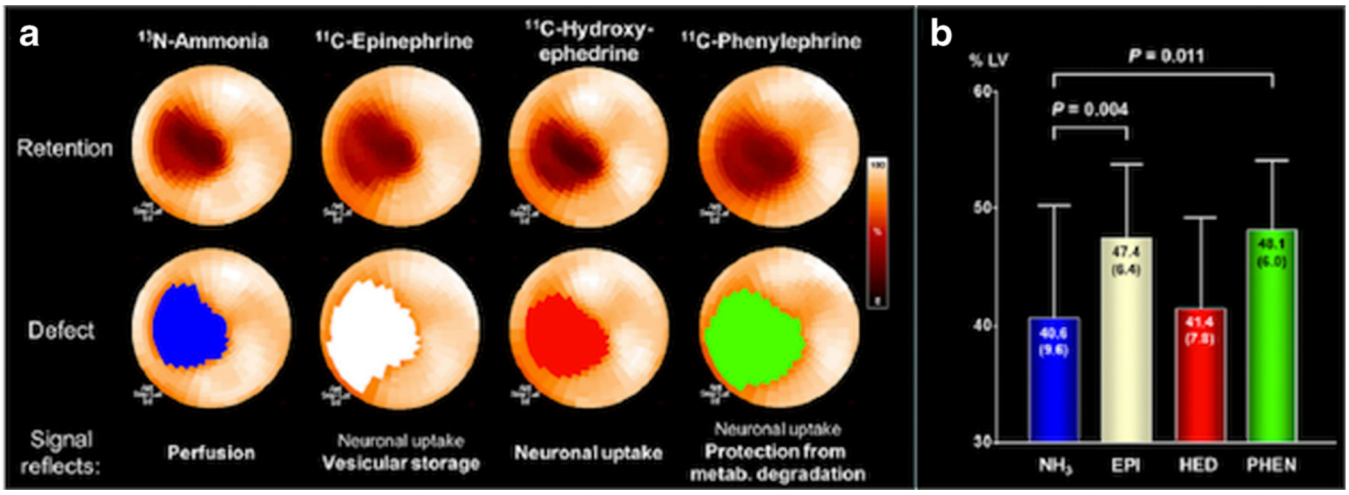

Fig. 3.

a Polar maps of a representative pig following an acute myocardial infarction of the mid-LAD territory using multiple radiolabeled catecholamines. b Bar graphs depicting the significant differences between the ^{13}N-ammonia defect area as a percentage of the total LV compared to the ^{11}C-epinephrine and ^{11}C-phenylephrine defect areas. There were no significant differences between the defect area of ^{13}N-ammonia and ^{11}C-HED and between the ^{11}C-epinephrine and ^{11}C-phenylephrine defect areas. *N* = 13 pigs. *Ant* anterior, *EPI* epinephrine, *HED* hydroxyephedrine, *inf inferior, lat* lateral, *metab*. metabolism, *NH*$_3$ ammonia, *PHEN* phenylephrine, *sep* septal (this research was originally published in *JNM* [60])

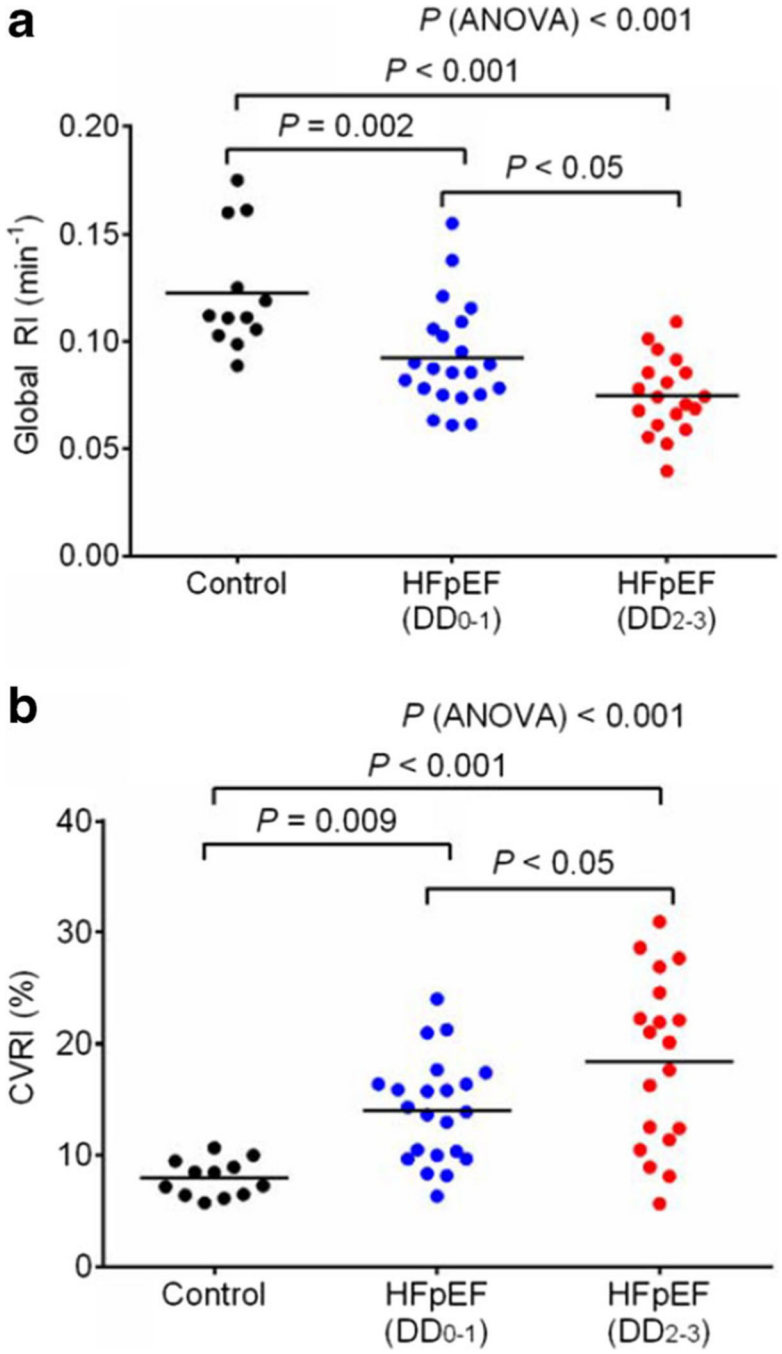

Fig. 4.

a Global retention index of ^{11}C-hydroxyephedrine determined from dynamic PET imaging in control subjects (n = 12) and patients with heart failure with preserved left ventricular ejection fraction (HFpEF) that have normal to mild diastolic dysfunction ($DD_{0–1}$; n = 22) and moderate to severe diastolic dysfunction ($DD_{2–3}$; n = 19). **b** Tracer uptake heterogeneity determined by the coefficient of variation in ^{11}C-hydroxyephedrine retention indices (RI/min) between left ventricular segments (17-segment model) in control subjects (n = 12) and in HFpEF patients with normal to mild diastolic dysfunction ($DD_{0–1}$; n = 22) and moderate

to severe diastolic dysfunction ($DD_{2–3}$; $n = 19$). Global retention index and tracer uptake heterogeneity were significantly different between controls and HFpEF patients and between HFpEF patients with normal to mild diastolic dysfunction and moderate to severe diastolic dysfunction. *RI/min* global retention index per minute, *HFpEF* heart failure with persevered ejection fraction, *DD* diastolic dysfunction, *0* no diastolic dysfunction, *1* mild diastolic dysfunction, *2* moderate diastolic dysfunction, *3* severe diastolic dysfunction, *CVRI%* coefficient of variance in global retention index per minute among left ventricular segments (this research was originally published in *JNM* [79••])

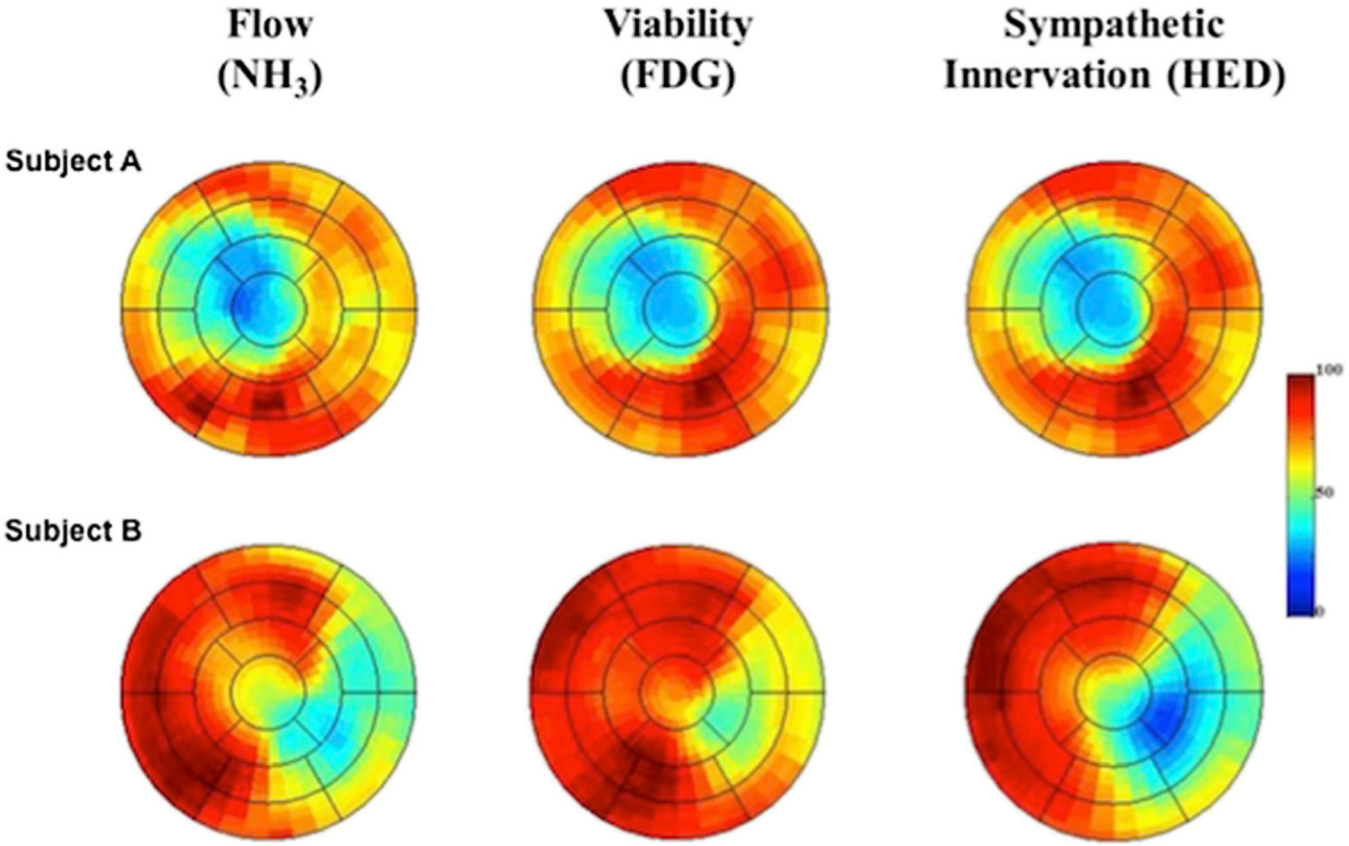

Fig. 5.

Polar maps of resting flow, myocardial viability, and sympathetic denervation measured with ^{13}N-ammonia ($^{13}NH_3$), insulin-stimulated ^{18}F-fluoro-2-deoxy-2-d-glucose (^{18}F-FDG), and ^{11}C-hydroxyephedrine (^{11}C-HED), respectively. Subject A shows the representative polar maps for a subject with matched reductions in flow, infarct volume, and sympathetic denervation volume. In contrast, *Subject B* shows representative polar maps in a subject developing sudden cardiac arrest showing larger denervation volume than infarct volume. In addition, this patient presents with reduced flow in areas of viable myocardium (preserved ^{18}F-FDG uptake) indicating areas of hibernating myocardium. *Ant* anterior, *INF* inferior, *LAT* lateral, *SEP* septal, *NH_3* ammonia, ^{18}F-FDG ^{18}F-fluoro-2-deoxy-2-d-glucose, *HED* hydroxyephedrine (reprinted from [51••])